mater.scichina.com link.springer.com

Published online 21 November 2023 | https://doi.org/10.1007/s40843-023-2630-1
Sci China Mater 2023, 66(12): 4615–4621

A novel rechargeable aqueous bismuth-air battery

Xiangran Cheng, Yi Jiang, Jiahe Qu, Chuanfa Li, Kun Zhang, Yanan Zhang, Bingjie Wang* and Huisheng Peng*

ABSTRACT Aqueous metal-air batteries own the merits of high theoretical energy density and high safety, but suffer from electrochemical irreversibility of metal anodes (e.g., Zn, Fe, Al, and Mg) and chemical instability of alkaline electrolytes to atmospheric CO_2. Here, we firstly design a rechargeable bismuth (Bi)-air battery using the non-alkaline bismuth triflate ($Bi(OTf)_3$) aqueous electrolyte. Benefitting from the three-electron reaction and the high potential of +0.32 V *vs.* standard hydrogen electrode, the Bi metal anode delivers a high capacity of 383 mA h g^{-1} and good stability for 1000 cycles with a Coulombic efficiency of 99.6% in the $Bi(OTf)_3$ electrolyte, without corrosion, passivation and hydrogen evolution reaction. Furthermore, the non-alkaline Bi-air battery achieves long-term operation stability (>200 h) in ambient air with the reversible formation/decomposition of bismuth trioxide (Bi_2O_3). This work sheds new light on the exploration of novel aqueous metal-air batteries as safe and stable power supply systems.

Keywords: metal-air battery, bismuth anode, non-alkaline electrolyte, cycling stability

INTRODUCTION

The emerging applications of batteries in electrified transportation and energy storage demand high energy density, low cost, and increased safety [1–5]. Aqueous metal-air batteries are considered as a promising power source owing to the high theoretical energy density and free-oxygen fuel from atmosphere [6–9]. To date, several aqueous metal-air batteries using zinc (Zn), magnesium (Mg), aluminum (Al), or iron (Fe) as the anode have been reported [10–13]. Unfortunately, these metal-air batteries still face the challenges of poor reversibility of metal anode and instability of alkaline electrolyte towards ambient CO_2. As presented in Fig. 1a, the aforementioned metal anodes have lower potentials than standard hydrogen electrode (SHE), and usually face inevitable corrosion, passivation and hydrogen evolution reaction (HER) in aqueous electrolytes, resulting in low Coulombic efficiency (CE) and short cycling life (Fig. S1) [13–15]. Besides, the most commonly used alkaline electrolytes (typically 30 wt% KOH) are limited by high causticity and fast carbonation in ambient air, causing undesirable electrolyte degradation and thereby inhibiting their use for prolonged operation [16–19]. Therefore, it is important to explore novel non-alkaline metal-air batteries to achieve long-term stability in ambient air.

Herein, we report a rechargeable bismuth (Bi)-air battery with non-alkaline bismuth triflate ($Bi(OTf)_3$) aqueous electrolyte (Fig. 1b). Owing to the three-electron redox reaction and high potential of +0.32 V *vs.* SHE, Bi metal anode exhibits a high capacity of 383 mA h g^{-1} (3748 mA h cm^{-3}) and good reversibility over 1000 cycles with high CE of 99.6% in $Bi(OTf)_3$ electrolyte, avoiding severe passivation and HER. The non-alkaline Bi-air batteries with $Bi(OTf)_3$ electrolyte are further constructed based on the redox mechanism of $4Bi + 3O_2 \leftrightarrow 2Bi_2O_3$, which deliver a good cycling performance for 200 h in ambient air. The novel Bi-air battery with long lifetime and high safety could inspire new development in aqueous rechargeable batteries.

EXPERIMENTAL SECTION

Preparation of electrolytes

Bismuth trifluoromethanesulfonate ($Bi(OTf)_3$) was purchased from Adamas. The electrolytes were prepared by dissolving the calculated amounts of the salts in deionized water according to the molarity (mol L^{-1}). Unless specific noted, the 1 mol L^{-1} $Bi(OTf)_3$ aqueous solution was used as electrolytes for the Bi-air batteries.

Preparation of bismuth anode

The Bi metal electrode was prepared by mixing 80 wt% bismuth powder (99.9999%, Adamas), 10 wt% carbon black (Super P® Li, Imerys) and 10 wt% poly(vinylidene) fluoride (HSV900, Arkema) binder in *N*-methyl-2-pyrrolidone (99.0%, Sinopharm). The slurry mixture was then coated on carbon paper (100 μm thick, HCP010, CeTech) with a designed mass loading of ~10 mg cm^{-2}. After coating, the electrodes were vacuum dried at 60°C for 24 h.

Preparation of air cathode

In a typical preparation of the air cathode, 40 mg Pt/C (20 wt% Pt, Suzhou Sinero technology Co., Ltd.) and 80 μL Nafion solution (10 wt%, D1020, DuPont) were dispersed in 10 mL ethanol (99.5%, Adamas). The as-obtained solution was dropped onto the gas diffusion layer (GDL39BC, SIGRACET). After coating, the air cathode was dried at room temperature for 24 h to remove the ethanol. The loading of catalyst was 1 mg cm^{-2}.

Cell assembly

C||Bi cells were assembled using carbon paper, Bi anode and

State Key Laboratory of Molecular Engineering of Polymers, Department of Macromolecular Science and Laboratory of Advanced Materials, Fudan University, Shanghai 200438, China
* Corresponding authors (emails: wangbingjie@fudan.edu.cn (Wang B); penghs@fudan.edu.cn (Peng H))

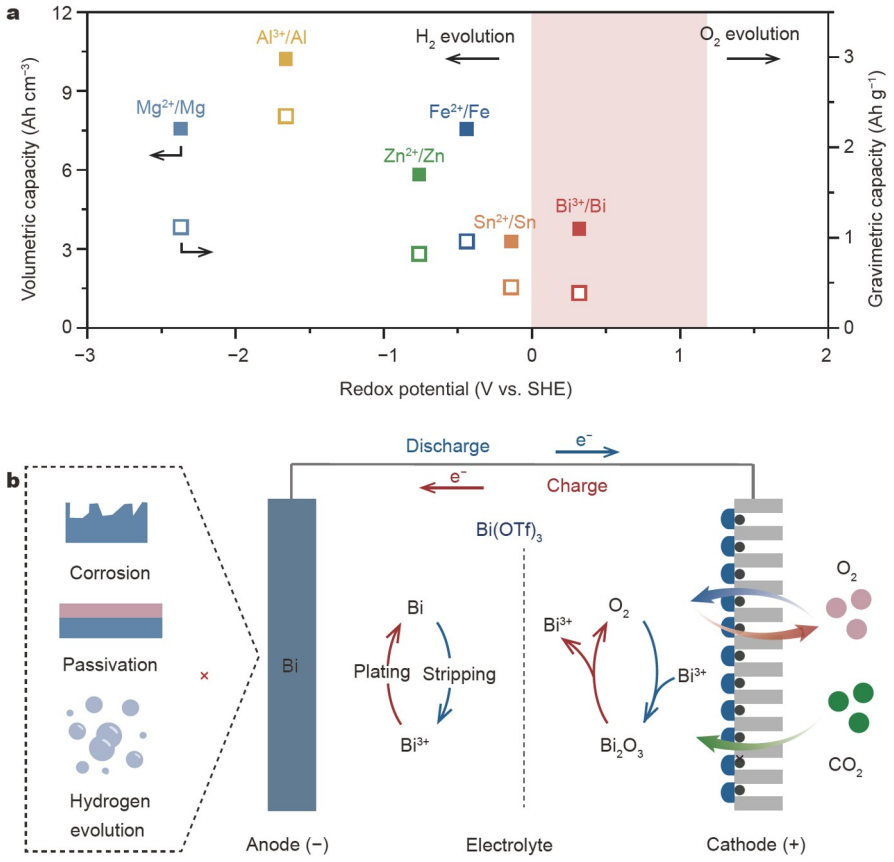

Figure 1 Rechargeable Bi-air battery using the non-alkaline 1 mol L^{-1} $Bi(OTf)_3$ aqueous electrolyte. (a) Redox potentials and theoretical specific capacities of the Bi anode and other reported metal anodes in metal-air batteries. (b) Reaction mechanism of the Bi-air battery using the non-alkaline $Bi(OTf)_3$ aqueous electrolyte based on the formation/decomposition of Bi_2O_3 on the cathode and the Bi stripping/plating on the anode.

1 mol L^{-1} $Bi(OTf)_3$ aqueous electrolyte and glass fiber (Whatman® GF/A) separator. Symmetric cells from Bi electrodes were assembled with 1 mol L^{-1} $Bi(OTf)_3$ aqueous electrolyte and glass fiber separator. Each symmetric cell contained ~100 μL electrolyte. The Bi-air battery was assembled in meshed CR2032 coin cells, where a Bi anode and the coated side of air cathode were stacked face-to-face with separator impregnated with 200 μL electrolyte in the middle. Glass fiber and Nafion® 117 membrane were used as the separators.

Materials characterization

Cells after electrochemical tests were disassembled in the ambient air. The discharged/charged air cathodes and Bi anodes were rinsed with deionized water for three times and then dried at room temperature for 24 h before measurements. X-ray diffraction (XRD) patterns were conducted on Bruker D8 Advance diffractometer with Ni filtered Cu Kα radiation. Scanning electron microscopy (SEM) was performed on a Zeiss Gemini SEM500 FESEM at 5 kV. Energy dispersive X-ray spectroscopy (EDS) investigations were performed using Aztec X-Max Extreme EDS. Transmission electron microscopy (TEM) was taken on JEOL JEM-2100F operated at 200 kV.

Electrochemical measurements

Cyclic voltammetry (CV) and linear sweep voltammetry (LSV) tests were carried out on a METROHM Autolab PGSTAT302N electrochemical workstation. The electrochemical impedance spectroscopy (EIS) test was carried out on a CHI 660D electrochemical workstation with a frequency range from 10^{-2} to 10^5 Hz and an amplitude of 5 mV. The open-circuit potential was set as the initial voltage. Galvanostatic cycling experiments were performed on the Land Battery Test System. The areal current density and areal capacity were calculated based on the Bi anode (1 cm^2).

RESULTS AND DISCUSSION

Properties of non-alkaline $Bi(OTf)_3$ electrolyte

For the construction of rechargeable Bi-air batteries, it is significant to prepare non-alkaline electrolytes that are compatible with both air cathode and Bi anode, and stable to ambient CO_2. Typically, Bi^{3+} can serve as the charge carrier for Bi-based batteries, which can be directly obtained *via* dissolving metal salts into aqueous solutions. However, most Bi(III) salts, such as bismuth sulfate ($Bi_2(SO_4)_3$), bismuth chloride ($BiCl_3$), bismuth acetate ($Bi(CH_3COO)_3$), and bismuth nitrate ($Bi(NO_3)_3$), undergo hydrolysis and form precipitates in the presence of water [20–22]. In contrast, $Bi(OTf)_3$ exhibits high solubility in water, because it hydrolyzes to generate trifluoromethanesulfonic acid (CF_3SO_3H, $pK_a = -14.7 \pm 2.0$), a superacid strong enough (HCl, $pK_a = -5.9 \pm 0.4$) to inhibit the hydrolysis of Bi^{3+} (Fig. S2) [23]. And the pH of 1 mol L^{-1} $Bi(OTf)_3$ aqueous electrolyte was measured as 0.58 (Fig. S3). $Bi(OTf)_3$ aqueous solution (1 mol L^{-1}) was therefore used as the electrolyte. The electro-

chemical stability window of the obtained electrolyte was evaluated using LSV on carbon paper electrodes with a scan rate of 0.5 mV s^{-1} (Fig. S4a). This aqueous electrolyte exhibited a high electrochemical stability up to ~1.5 V. The ionic conductivity of the electrolyte was measured as ~10.3 mS cm^{-1}, providing good ionic transport capability (Fig. S4b).

Electrochemical performance of Bi anode

The Bi electrode was prepared by coating Bi powder slurries on carbon paper substrate as the current collector. As shown in Fig. S5, Bi was homogeneously distributed on the carbon paper substrate. The XRD peaks can be indexed to rhombohedral Bi (JCPDS card No. 00-044-1246) (Fig. S6).

The plating/stripping behavior of Bi in the 1 mol L^{-1} $Bi(OTf)_3$ electrolyte was studied using CV with a scan rate of 0.5 mV s^{-1} in a three-electrode test system, where carbon paper served as the working electrode and Bi served as the counter and reference electrodes. As shown in Fig. 2a, obvious plating/stripping processes of Bi anode were observed, indicating the feasibility of a reversible reaction, i.e., Bi ↔ Bi^{3+} + $3e^-$. It is worth noting that Bi deposition occurred at −0.05 V *vs.* Bi^{3+}/Bi, which is higher than the SHE (−0.32 V *vs.* Bi^{3+}/Bi), thereby effectively avoiding undesired corrosion and hydrogen evolution in the $Bi(OTf)_3$ electrolyte (Fig. S7). To further evaluate the efficiency of Bi plating/stripping in the $Bi(OTf)_3$ electrolyte, C||Bi cells were subjected to discharge/charge cycles at 0.1 mA cm^{-2} and 0.1 mA h cm^{-2}. As shown in Fig. 2b, c and Fig. S8, the CE calculated from the ratio of the stripped Bi to plated Bi in each cycle remained at high level of 99.6% after 1000 cycles. Bi anode still retained the high capacities of 383 mA h g^{-1} and 3748 mA h cm^{-3} after cycling, approaching to its theoretical capacities (385 mA h g^{-1}, 3762 mA h cm^{-3}). Moreover, when tested at a higher current density of 0.5 mA cm^{-2}, the Bi anode can work stably for 1000 cycles, attributed to the high reversibility of Bi anode (Fig. S9). Even at 1 mA cm^{-2} with the capacity of 2 mA h cm^{-2}, Bi plating/stripping remained a high CE of 98.8%, indicating good rate capability (Fig. S10).

The cycling stability of Bi metal anode was further investigated in Bi||Bi symmetric cells using the $Bi(OTf)_3$ electrolyte. The voltage of repeated plating/stripping of Bi anode showed a low

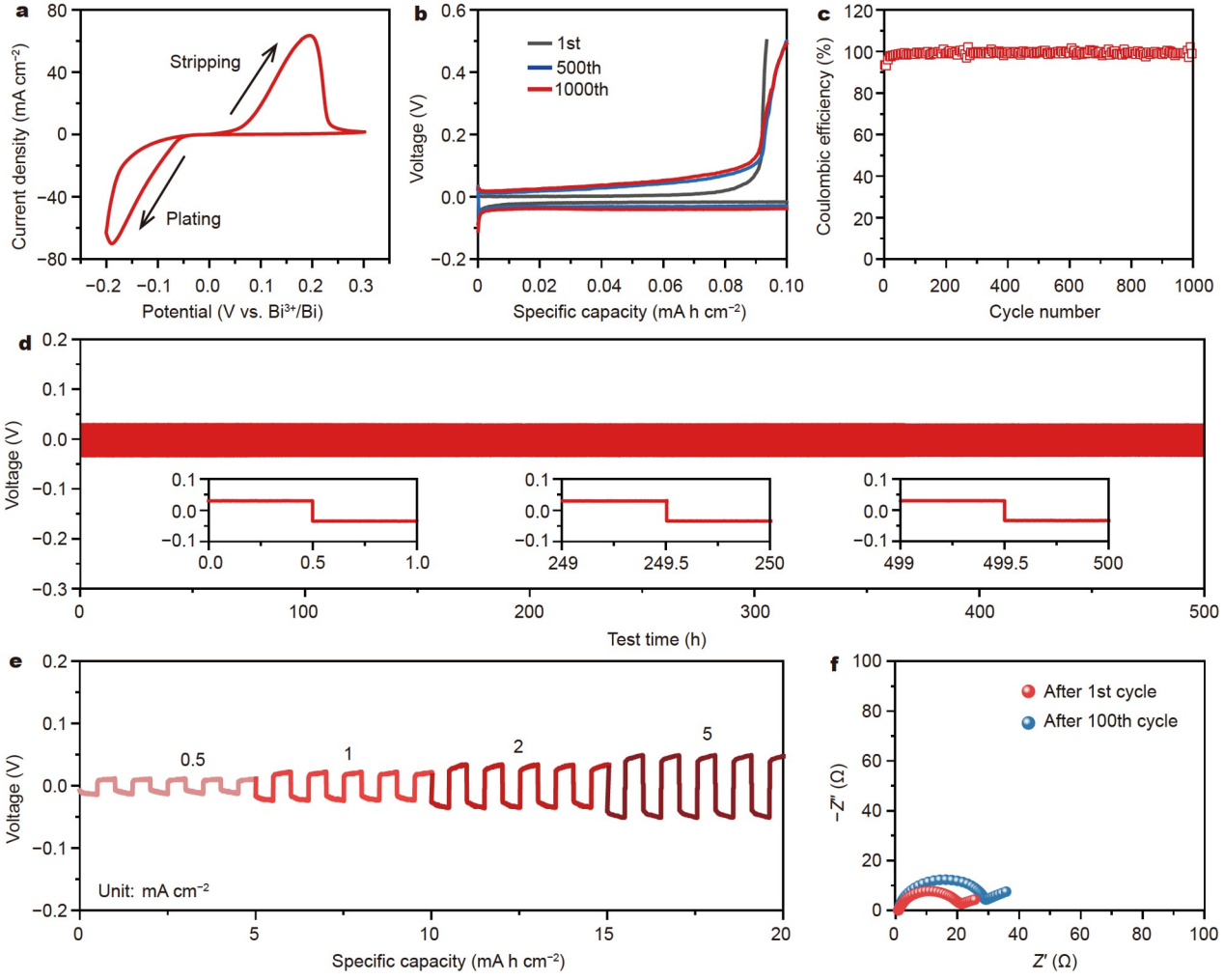

Figure 2 Electrochemical performance of the Bi anode in the 1 mol L^{-1} $Bi(OTf)_3$ electrolyte. (a) CV curve of the Bi anode at 0.5 mV s^{-1} in a three-electrode cell using the 1 mol L^{-1} $Bi(OTf)_3$ electrolyte. Carbon paper was used as the working electrode, and Bi metal plates were used as the counter electrode and reference electrode. (b) Voltage profiles of the C||Bi cells using the $Bi(OTf)_3$ electrolyte at 0.1 mA cm^{-2} with the capacity of 0.1 mA h cm^{-2} and the cut-off voltage of 0.5 V. (c) Corresponding CE of Bi plating/stripping in the $Bi(OTf)_3$ electrolyte. (d) Cycling performance of Bi||Bi symmetric cells using the 1 mol L^{-1} $Bi(OTf)_3$ electrolyte at 1 mA cm^{-2} with the capacity of 0.5 mA h cm^{-2}. (e) Rate performance of Bi||Bi symmetric cells at current densities ranging from 0.5 to 5 mA cm^{-2}. (f) EIS curves of the Bi||Bi symmetric cells after the 1st cycle and 100th cycle at 1 mA cm^{-2} with the capacity of 0.5 mA h cm^{-2}.

overpotential of about 65 mV without fluctuation for 500 cycles at 1 mA cm^{-2} for 0.5 mA h cm^{-2}, demonstrating excellent interfacial stability (Fig. 2d). When tested at current densities from 0.5 to 5 mA cm^{-2}, the overpotential of the Bi electrode only marginally increased at high rates, indicating favorable Bi plating/stripping kinetics (Fig. 2e). The rising voltage plateaus can be attributed to the electrode material becoming loose in structure and exfoliated from electrode during plating and stripping processes, resulting in the increased internal resistance and polarization of the battery [24]. The EIS curves of Bi||Bi symmetric cells also revealed that the charge transfer resistance increased slightly from 20 to 28 Ω after 100 cycles at 1 mA cm^{-2} and 0.5 mA h cm^{-2}, indicating high reversibility and good interfacial stability (Fig. 2f). Furthermore, Bi electrodes were extracted from cycled Bi||Bi symmetric cells for characterization. As shown by the XRD pattern, the dominant peaks of Bi were observed on cycled Bi metal electrodes, indicating no passivation layer formation (Fig. S11a). SEM image also showed that Bi electrode maintained smooth surface and dendrite-free deposition (Fig. S11b).

Electrochemical performance of the Bi-air batteries

Inspired by the high performance of Bi anode in the Bi(OTf)$_3$ electrolyte, the non-alkaline Bi-air batteries were further assembled. CV tests were performed on Bi-air batteries to investigate the electrochemical behavior under ambient air and Ar atmosphere at a scan rate of 0.5 mV s^{-1}. As presented in Fig. 3a, the CV curve of Bi-air batteries under air atmosphere showed that a cathodic peak started at ~0.5 V corresponding to the oxygen reduction reaction (ORR) and an anodic peak started at ~1.0 V corresponding to the oxygen evolution reaction (OER). Considering the small electrode polarization of Bi anode in Fig. 2a, the high overpotential in Bi-air batteries was primarily attributed to electrochemical reaction occurring at the air cathode. Under Ar atmosphere, only a small capacitive response current was still observed due to the electrical double-layer capacitance of the porous carbon on the electrodes [25]. Besides, galvanostatic discharge performance of Bi-air batteries was also studied at 0.1 mA cm^{-2} with the cut-off voltage of 0 V (Fig. 3b). The non-alkaline Bi-air batteries using 1 mol L^{-1} Bi(OTf)$_3$ electrolyte presented a well-defined discharge plateau at ~0.5 V and delivered a capacity of 2.0 mA h cm^{-2}, achieving a high Bi utilization of ~65%. Under Ar atmosphere, the Bi-air batteries can hardly output capacity and the voltage quickly dropped to 0 V, demonstrating O_2 was the active species involved in the cathode reaction. The Bi-air batteries using 6 mol L^{-1} KOH electrolyte were also investigated for comparison. In sharp contrast, the Bi-air batteries displayed fluctuating discharge voltage with a lower capacity of 1.2 mA h cm^{-2} in 6 mol L^{-1} KOH electrolyte, which may be due to the strong corrosive nature of the concentrated alkaline electrolyte (Figs S12 and S13).

Galvanostatic discharge/charge investigation of Bi-air batteries was tested at the current density of 0.2 mA cm^{-2} with the capacity of 1 mA h cm^{-2}. The typical discharge/charge profiles of Bi-air batteries displayed a stable discharge plateau at ~0.45 V and a charge plateau at ~1.0 V, which were consistent with the cathodic and anodic peaks in the CV investigation (Fig. 3c). Furthermore, Bi-air batteries were cycled at a current density of 0.1 mA cm^{-2} with 0.5 h discharge and charge per cycle under ambient air atmosphere. As presented in Fig. 3d and Fig. S14, Bi-air batteries showed an excellent cycling stability for 200 h with

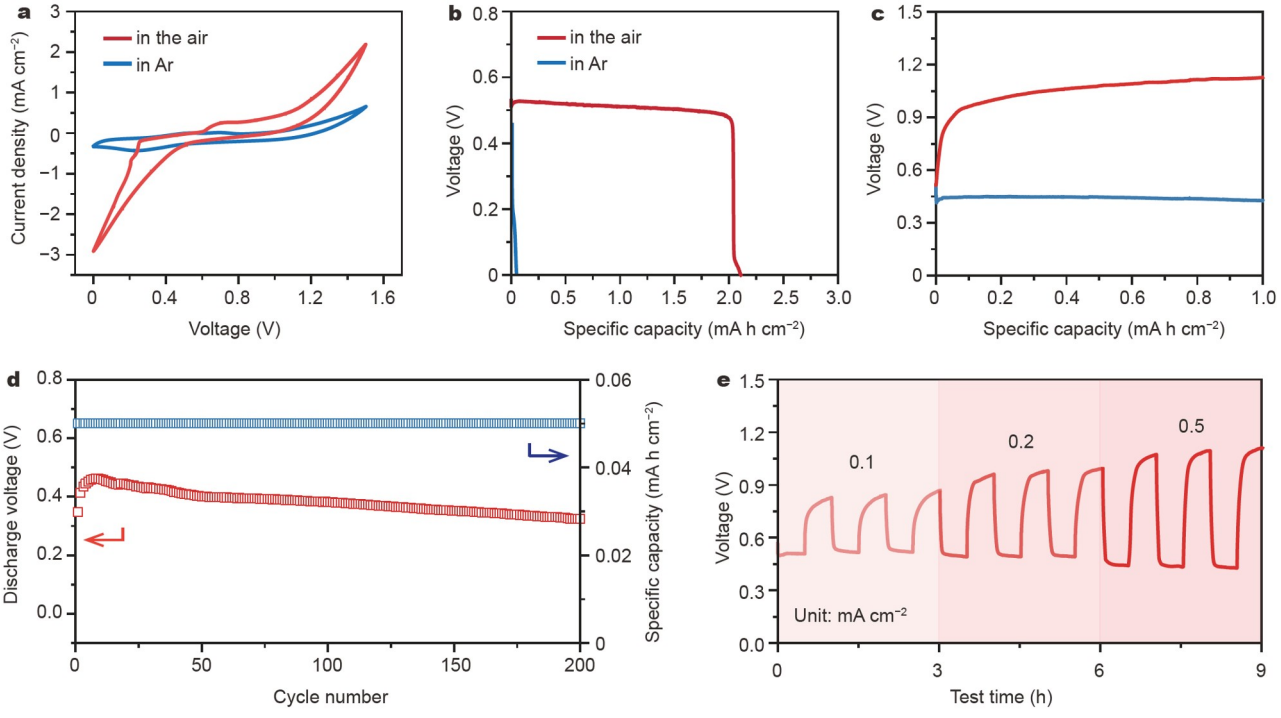

Figure 3 Electrochemical performance of the Bi-air batteries using the 1 mol L^{-1} Bi(OTf)$_3$ aqueous electrolyte. (a) CV curves of the Bi-air batteries under the ambient air and Ar atmosphere with a scan rate of 0.5 mV s^{-1}. (b) Galvanostatic discharge curves of the Bi-air batteries in the ambient air and Ar atmosphere at 0.1 mA cm^{-2} with the cut-off voltage of 0 V. (c) Galvanostatic discharge/charge profiles of the Bi-air batteries in the ambient air at 0.2 mA cm^{-2} with the capacity of 1 mA h cm^{-2}. (d) Long-term cycling performance of the Bi-air batteries at 0.1 mA cm^{-2}. (e) Rate performance of the Bi-air batteries at current densities ranging from 0.1 to 0.5 mA cm^{-2}.

no major polarization increase, which was attributed to the reduced parasite reactions such as anode passivation and electrolyte carbonization. To highlight the improved cycling stability by non-alkaline electrolyte, Bi-air batteries using $Bi(OTf)_3$ and KOH electrolyte were cycled in a constant capacity of 0.1 mA h cm^{-2} at 0.1 mA cm^{-2} under ambient air atmosphere. As shown in Fig. S15, Bi-air batteries using $Bi(OTf)_3$ electrolytes exhibited excellent cycling stability within 90 cycles (180 h). In comparison, Bi-air batteries using KOH electrolyte presented sudden polarization increase indicating battery failure after only three cycles. The air tolerance of Bi-air batteries with non-alkaline $Bi(OTf)_3$ electrolyte is beneficial for practical applications, because complicated and costly cell design providing pure oxygen atmosphere are not necessary.

The rate performance of the Bi-air batteries was further examined at different current densities with a fixed time of 1 h per cycle (Fig. 3f). A slightly increasing polarization was observed when the current increased from 0.1 to 0.5 mA cm^{-2} and the capacity increased from 0.05 to 0.25 mA h cm^{-2}. When cycled at a higher current density of 0.5 mA cm^{-2}, the Bi-air batteries also delivered stable cycling performance for 60 h in ambient air (Fig. S16).

Reaction mechanism of the Bi-air batteries

To reveal the reaction mechanism, the air cathode and Bi anode were extracted from Bi-air batteries using $Bi(OTf)_3$ electrolyte after discharging/charging at 0.1 mA cm^{-2} for 10 h (Fig. S17). As shown in Fig. 4a, XRD patterns of discharged air cathode were indexed to cubic bismuth trioxide (Bi_2O_3) (JCPDS PDF 01-074-1375), besides the peaks of the polyvinylidene fluoride (PVDF) binder and carbon from the pristine carbon-based air cathode. As observed from SEM images in Fig. 4b and Fig. S18, the discharged product in the air cathode presented cubic particle morphology within the scale of a few hundred nanometers. The TEM lattice images of the discharged air cathode confirmed the lattice spacing of 0.407 nm for (211) plane of Bi_2O_3 (JCPDS PDF 01-074-1375) (Fig. 4d, e) [26]. Besides, the corresponding EDS mappings of the discharged cathode showed the discharge product consisted of Bi and O (Fig. 4f and Fig. S19). The formation of Bi_2O_3 during discharge can be attributed to the ORR

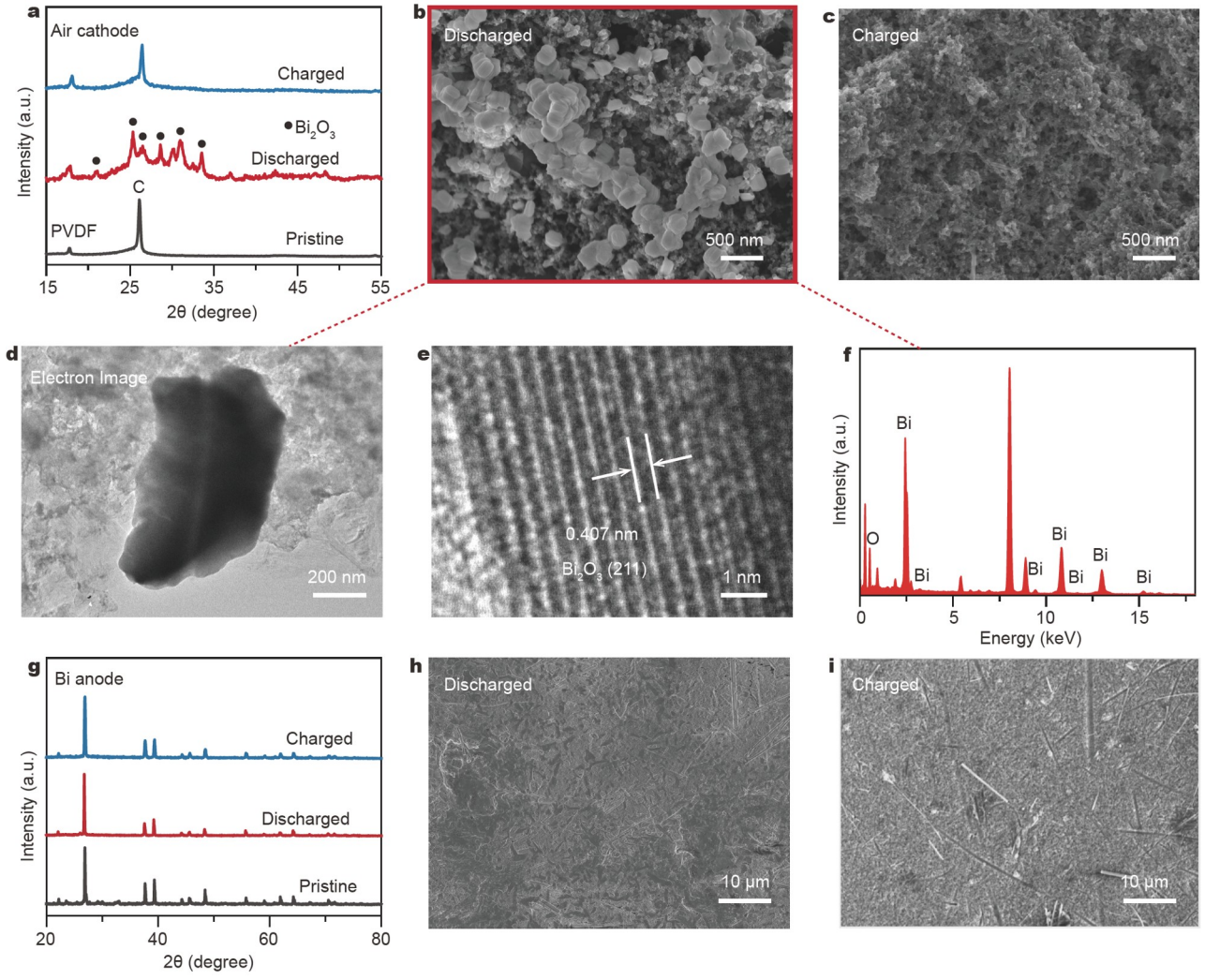

Figure 4 Electrochemical reaction mechanisms of the Bi-air batteries using the 1 mol L^{-1} $Bi(OTf)_3$ electrolyte. (a) XRD patterns of the air cathodes at the pristine, discharged and recharged states, respectively. (b, c) SEM images of the air cathode at the discharged and recharged states, respectively. (d–f) TEM images and the corresponding EDS profiles of the discharged air cathode. (g) XRD patterns and (h, i) SEM images of the Bi anodes obtained from the Bi-air batteries after discharge and charge processes, respectively.

reaction at the cathode, which increased the pH of the electrolyte at the cathode, leading to the hydrolysis of Bi^{3+} to Bi_2O_3 [27]. Upon recharge, all the XRD peaks associated with Bi_2O_3 disappeared, and no Bi_2O_3 particle was observed by SEM, suggesting the reversible formation/decomposition of Bi_2O_3 at the air cathode (Fig. 4a, c).

The redox process of the Bi anode was also confirmed. After the discharge/charge process, the distinct XRD peaks of Bi were observed on the Bi metal anode without other by-products, indicating the absence of corrosion and passivation on the Bi anode (Fig. 4g). The SEM images revealed that there was no obvious change in the morphology of Bi anode after discharging and charging processes, respectively (Fig. 4h, i). Combining the formation/decomposition of Bi_2O_3 on the air cathode, Bi plating/stripping on the anode side, the reaction equation of the Bi-air batteries using $Bi(OTf)_3$ electrolyte should be expressed as $4Bi + 3O_2 \leftrightarrow 2Bi_2O_3$ (Fig. S20). The Bi-air batteries also exhibited high reversibility after 200-h operation in ambient air at the current density of 0.1 mA cm^{-2}. As presented in the XRD patterns, only minor Bi_2O_3 was observed on the air cathode after 200th recharging process (Fig. S21). For cycled Bi metal anode, the dominant peaks of Bi remained, while minor Bi_2O_3 appeared due to the chemical oxidation by the dissolved O_2 in electrolytes (Fig. S22).

CONCLUSIONS

In summary, a novel rechargeable Bi-air battery using a non-alkaline $Bi(OTf)_3$ electrolyte was demonstrated, which exhibited a long-term stability when operated in ambient air. Due to the reversible three-electron transfer and the high hydrogen overpotential, the Bi metal anode delivered a high capacity of 383 mA h g^{-1} and good reversibility over 1000 cycles with the CE of 99.7% in $Bi(OTf)_3$ electrolyte, avoiding passivation and hydrogen evolution side reactions. Furthermore, the Bi-air battery was assembled and can stably work for 200 cycles in ambient air, benefitting from the chemical stability of the non-alkaline $Bi(OTf)_3$ electrolyte against ambient CO_2. The unique battery chemistry with reversible formation and decomposition of Bi_2O_3 was also revealed using electrochemical and analytical techniques. This novel non-alkaline Bi-air battery provides a new idea for exploring safe and stable energy storage systems.

Received 16 August 2023; accepted 25 September 2023; published online 21 November 2023

1 Zhu Z, Jiang T, Ali M, *et al.* Rechargeable batteries for grid scale energy storage. Chem Rev, 2022, 122: 16610–16751
2 Cano ZP, Banham D, Ye S, *et al.* Batteries and fuel cells for emerging electric vehicle markets. Nat Energy, 2018, 3: 279–289
3 Liang Y, Yao Y. Designing modern aqueous batteries. Nat Rev Mater, 2023, 8: 109–122
4 Duffner F, Kronemeyer N, Tübke J, *et al.* Post-lithium-ion battery cell production and its compatibility with lithium-ion cell production infrastructure. Nat Energy, 2021, 6: 123–134
5 Chao D, Zhou W, Xie F, *et al.* Roadmap for advanced aqueous batteries: From design of materials to applications. Sci Adv, 2020, 6: eaba4098
6 Cheng F, Chen J. Metal-air batteries: From oxygen reduction electrochemistry to cathode catalysts. Chem Soc Rev, 2012, 41: 2172–2192
7 Kwak WJ, Rosy WJ, Sharon D, *et al.* Lithium-oxygen batteries and related systems: Potential, status, and future. Chem Rev, 2020, 120: 6626–6683
8 Fu J, Cano ZP, Park MG, *et al.* Electrically rechargeable zinc-air batteries: Progress, challenges, and perspectives. Adv Mater, 2017, 29: 1604685
9 Rahman MA, Wang X, Wen C. High energy density metal-air batteries: A review. J Electrochem Soc, 2013, 160: A1759–A1771
10 Sun W, Wang F, Zhang B, *et al.* A rechargeable zinc-air battery based on zinc peroxide chemistry. Science, 2021, 371: 46–51
11 Li L, Chen H, He E, *et al.* High-energy-density magnesium-air battery based on dual-layer gel electrolyte. Angew Chem Int Ed, 2021, 60: 15317–15322
12 Wu S, Hu S, Zhang Q, *et al.* Hybrid high-concentration electrolyte significantly strengthens the practicability of alkaline aluminum-air battery. Energy Storage Mater, 2020, 31: 310–317
13 Wu X, Markir A, Xu Y, *et al.* A rechargeable battery with an iron metal anode. Adv Funct Mater, 2019, 29: 1900911
14 Sui Y, Ji X. Anticatalytic strategies to suppress water electrolysis in aqueous batteries. Chem Rev, 2021, 121: 6654–6695
15 Kim H, Jeong G, Kim YU, *et al.* Metallic anodes for next generation secondary batteries. Chem Soc Rev, 2013, 42: 9011–9034
16 Sun W, Küpers V, Wang F, *et al.* A non-alkaline electrolyte for electrically rechargeable zinc-air batteries with long-term operation stability in ambient air. Angew Chem, 2022, 134: e202207353
17 Liu Q, Pan Z, Wang E, *et al.* Aqueous metal-air batteries: Fundamentals and applications. Energy Storage Mater, 2020, 27: 478–505
18 Wang ZL, Xu D, Xu JJ, *et al.* Oxygen electrocatalysts in metal-air batteries: From aqueous to nonaqueous electrolytes. Chem Soc Rev, 2014, 43: 7746–7786
19 Chang Z, Yang Y, Li M, *et al.* Green energy storage chemistries based on neutral aqueous electrolytes. J Mater Chem A, 2014, 2: 10739–10755
20 Granér F, Sillén LG. Hydrolysis of Bi^{3+}. Oxygen bridging—A new type of ionic equilibrium. Nature, 1947, 160: 715–716
21 Miersch L, Rüffer T, Schlesinger M, *et al.* Hydrolysis studies on bismuth nitrate: Synthesis and crystallization of four novel polynuclear basic bismuth nitrates. Inorg Chem, 2012, 51: 9376–9384
22 Mokrai R, Barrett J, Apperley DC, *et al.* Tweaking the charge transfer: Bonding analysis of bismuth(III) complexes with a flexidentate phosphane ligand. Inorg Chem, 2020, 59: 8916–8924
23 Trummal A, Lipping L, Kaljurand I, *et al.* Acidity of strong acids in water and dimethyl sulfoxide. J Phys Chem A, 2016, 120: 3663–3669
24 Zhang H, Liu Q, Zheng D, *et al.* Oxygen-rich interface enables reversible stibium stripping/plating chemistry in aqueous alkaline batteries. Nat Commun, 2021, 12: 14
25 Ji H, Zhao X, Qiao Z, *et al.* Capacitance of carbon-based electrical double-layer capacitors. Nat Commun, 2014, 5: 3317
26 Hu ZT, Chen B, Lim TT. Single-crystalline $Bi_2Fe_4O_9$ synthesized by low-temperature co-precipitation: Performance as photo- and Fenton catalysts. RSC Adv, 2014, 4: 27820–27829
27 Su H, Cao S, Xia N, *et al.* Controllable growth of Bi_2O_3 with rod-like structures *via* the surfactants and its electrochemical properties. J Appl Electrochem, 2014, 44: 735–740

Acknowledgements This work was financially supported by the Science and Technology Commission of Shanghai Municipality (STCSM, 21511104900 and 20JC1414902) and the National Natural Science Foundation of China (52222310).

Author contributions Cheng X performed most experiments and characterizations and prepared the manuscript. Cheng X, Wang B, and Peng H discussed the results and co-wrote the manuscript. Jiang Y, Qu J, Li C, Zhang K and Zhang Y assisted in some experimental measurements and manuscript correction. All authors contributed to the general discussion.

Conflict of interest The authors declare that they have no conflict of interest.

Supplementary information Supporting data are available in the online version of the paper.

Xiangran Cheng is currently a PhD student at the Department of Macromolecular Science, Fudan University. She received her BS degree in chemical engineering from Dalian University of Technology in 2019. Her work focuses on electrode materials, metal-air batteries, and their applications in flexible energy storage systems.

Bingjie Wang is an associate professor at the Laboratory of Advanced Materials, Fudan University. He received his BE degree in polymer materials and engineering from Sichuan University in 2009, and a PhD degree from Ningbo Institute of Materials Technology and Engineering, Chinese Academy of Sciences in 2014. His research centers on flexible energy storage devices.

Huisheng Peng is currently a university professor at the Department of Macromolecular Science and Laboratory of Advanced Materials, Fudan University. He received his BE degree in polymer materials from Donghua University in 1999, his MS degree in macromolecular chemistry and physics from Fudan University in 2003, and his PhD degree in chemical engineering from Tulane University in the USA in 2006. He then worked at Los Alamos National Laboratory before joining Fudan University in 2008. He focuses on the new direction of fiber electronics.

一种新型可充的水系铋-空气电池

程翔然, 姜怡, 屈佳禾, 李传发, 张琨, 张延安, 王兵杰*, 彭慧胜*

摘要 水系金属空气电池具有理论能量密度高、安全性高等优点，但受限于金属阳极(如锌、铁、铝、镁)的电化学不可逆性以及碱性电解质对大气中二氧化碳的化学不稳定性. 本工作首次设计了一种可充电的铋-空气电池，该电池使用了非碱性的三氟甲磺酸铋($Bi(OTf)_3$)水系电解质. 得益于三电子反应和相对于标准氢电极+0.32 V的高电位，铋金属负极具有383 mA h g^{-1}的高比容量和1000次循环的良好稳定性，以及99.6%高库仑效率. 铋金属负极在$Bi(OTf)_3$电解液中无腐蚀、钝化和析氢等副反应. 此外，非碱性的铋-空气电池通过三氧化二铋(Bi_2O_3)的可逆形成/分解，在环境空气中实现了长期运行稳定性(>200 h). 这项工作为探索新型水系金属空气电池作为安全稳定的电源系统提供了新思路.